A general framework for softening regularisation based on gradient elasticity

Antonio Rodríguez-Ferran[a,*], Terry Bennett[b], Harm Askes[b], Elena Tamayo-Mas[a]

[a] *Laboratori de Càlcul Numèric (LaCàN), Departament de Matemàtica Aplicada III, Universitat Politècnica de Catalunya, Barcelona, Spain*
[b] *University of Sheffield, Department of Civil and Structural Engineering, Sheffield, United Kingdom*

Abstract

A general non-local approach to regularise strain-softening continua is presented. The key idea is to introduce the gradient-type enrichment at the level of displacements (rather than some internal variable), so the model is formulated with two distinct displacement fields. In fact, gradient models based on two displacement fields are usual in non-local *elasticity*, where the goal is to avoid the shortcomings of classical (local) elasticity (i.e. strain singularities in statics, non-dispersive behaviour in dynamics). We show that such a gradient elasticity backbone model can be combined with any standard nonlinear constitutive driver to render a regularised model for softening inelasticity. To illustrate the generality of the approach, two prototype models (isotropic damage and von Mises plasticity) are discussed. The numerical examples show that the regularised models exhibit all of the desired features: mesh insensitivity, imperfection size insensitivity and description of size effects.

Keywords: regularisation, strain-softening, gradient elasticity, non-locality, internal length scale

*Corresponding author
Email address: antonio.rodriguez-ferran@upc.edu (Antonio Rodríguez-Ferran)
URL: www-lacan@upc.edu (Antonio Rodríguez-Ferran)

1. INTRODUCTION

Classical continuum theories are material models in which the stress is related to the strain or the stress rate related to the strain rate. Further derivatives (either spatial or temporal) are absent in the constitutive relations. These models do not include any information on the underlying microstructure of the material, and it is well known that they are not capable to describe realistically phenomena that are driven by physical processes in which the microstructure interacts with the macroscopic geometry and boundary conditions. Without attempting to be complete, a few examples of the anomalies are given of classical continuum descriptions for elasticity and inelasticity. Firstly, classical elasticity predicts singularities in stresses and strains at the tip of sharp cracks or at dislocations. This indicates that the usual definitions of stress and strain break down when used at very small levels of observation. Secondly, classical elasticity predicts a non-dispersive propagation of waves, whereas experiments conducted on heterogeneous materials show a dependence of the propagation characteristics (angular frequency, phase velocity) on the wave number, i.e. in reality wave propagation is dispersive. Thirdly, classical continua are not able to provide a mathematically well-posed problem in case the peak in the stress-strain curve is exceeded — a loss of uniqueness is observed and, correspondingly, numerical simulations exhibit a strong and unrealistic sensitivity to the used spatial discretisation. Finally, experiments indicate that the mechanical properties of proportionally scaled specimens of different size depend on the actual size of the specimen. These so-called "size effects" are not predicted by classical continua.

Thus, amendments to classical continuum descriptions are needed for applications in elasticity as well as inelasticity. A popular class of non-classical continua are the so-called *non-local continua*, in which the governing equations are extended with additional spatial averages (via integrals) or spatial derivatives of one or more variables. These additional terms are accompanied by additional material parameters which are normally expressed as *internal length scales*, and precisely these internal length scales are a manifestation of the microstructure that is lacking in classical continuum models. For a general overview of non-local continuum models, we refer to the reviews by Bažant and Jirásek (2002) and Aifantis (2003).

1.1. Computational aspects

In the computational mechanics community, many different implementations have been suggested during the last few decades for non-local continua. Two relevant issues, when considering non-local continuum models for finite element implementation, are (i) employing standard element-by-element assembly procedures or not, and (ii) the required continuity of the interpolation functions. Regarding the first issue, there is a certain drawback in using non-locality of the integral-type, as this class of models requires assembly of element contributions that go beyond the nearest neighbours. While this is not impossible (Jirásek and Patzak, 2002; Rodríguez-Ferran et al., 2004), nevertheless such procedures are not straightforwardly embedded in existing finite element software that is normally based on an element-by-element assembly of the tangent stiffness matrices (de Vree et al., 1995). In contrast, the differential nature of gradient-type non-locality combines naturally with finite element assembly procedures.

The second issue, that of continuity of the interpolants, is normally not relevant for the integral-type non-locality but may become problematic for classes of gradient enrichment where the governing partial differential equations are of the order four or higher. This can often be avoided in the formulation of gradient damage and gradient plasticity theories, but gradient elasticity theories are normally fourth-order differential equations and would, thus, require $\mathcal{C}^1$-continuity of the interpolations. Several strategies have been proposed to accomodate $\mathcal{C}^1$-continuous interpolations for gradient elasticity, including meshless methods (Askes and Aifantis, 2002; Tang et al., 2003), continuous/discontinuous Galerkin methods (Engel et al., 2002) or the simultaneous interpolation of multiple state variables (Shu et al., 1999; Amanatidou and Aravas, 2002; Askes and Gutierrez, 2006; Zervos, 2008). However, these strategies often lead to either an important increase in the number of degrees of freedom or to nodal connectivities that extend beyond the nearest neighbour, thus affecting element assembly procedures.

A competitive implementation strategy is based on the operator split of Ru and Aifantis, in which the fourth-order partial differential equations of gradient elasticity are split into two sets of second-order partial differential equations (Ru and Aifantis, 1993). The associated finite element implementations have also been pursued by (Tenek and Aifantis, 2002; Askes et al., 2008), and more recently the extension towards dynamics has been made by Askes et al. (2007). Interestingly, whereas the original splits of Ru and Aifantis were formulated for use in gradient elasticity, similar strategies of reformulation

into two sets of coupled second-order differential equations were suggested for gradient-enriched inelastic models (Rodríguez-Ferran et al., 2005; Jirásek and Marfia, 2005). As in the approach of Ru and Aifantis, the two sets of unknowns are two sets of displacements, one of which is local or unsmoothed and one of which is non-local or smoothed.

1.2. Towards a general formulation of gradient theories

The recent progress made in the implementation of various gradient-enriched theories using two distinct displacement fields as the primary unknowns has inspired to attempt a further unification of the various implementations of gradient theories. This is based on the following observations:

- Microstructural influences occur in elastic as well as inelastic stages of the loading process. Thus, it would be desirable to have a material model that is equipped with non-locality in both stages of loading;
- In certain earlier formulations of gradient theories, the non-locality was embedded within the nonlinear constitutive update, see for instance Muhlhaus and Aifantis (1991); de Borst and Muhlhaus (1992) as well as Ramaswamy and Aravas (1998a) and Ramaswamy and Aravas (1998b). For a straightforward coupling of non-locality with the various classical nonlinear material models that exist in the literature, it would be desirable if the non-locality does not interfere with the constitutive parts of the finite element package.

For these reasons, the aim is to formulate a general framework of non-local models of the gradient-type, whereby the gradient-enrichment affects the elastic parts as well as the inelastic parts of the response. Furthermore, in its implementation the formulation should exhibit a clear division between the non-locality and the (nonlinear) constitutive driver. In short, a gradient elasticity backbone model is combined with a standard constitutive driver.

1.3. Outline

The remainder of this paper is organised as follows. The general gradient-enriched model is presented in Section 2, first for elasticity and then for inelasticity. As prototype inelastic models, von Mises plasticity and isotropic damage will be used. The appropriate formats for softening regularisation are chosen based on the localisation analysis of Section 3. The finite element discretisation is described in Section 4. One- and two-dimensional numerical

examples are shown in Section 5. Two key features are analysed: regularisation of softening and modelling of size effects.The concluding remarks of Section 6 close the paper.

2. MODEL FORMULATION

In the 1990s, Aifantis and coworkers formulated a gradient elasticity theory whereby the stresses $\boldsymbol{\sigma}$ are not only related to the strains $\boldsymbol{\varepsilon}$ but also to the Laplacian of the strains (Aifantis, 1992; Altan and Aifantis, 1992; Ru and Aifantis, 1993):

$$\boldsymbol{\sigma} = \boldsymbol{C} : \left(\boldsymbol{\varepsilon} - \ell^2 \nabla^2 \boldsymbol{\varepsilon}\right) \tag{1}$$

where $\boldsymbol{C}$ is a fourth-order tensor with the elastic moduli and ℓ is an internal length scale. The infinitesimal strains equal, as usual, the symmetric gradient of the displacements $\boldsymbol{u}_g$, that is $\boldsymbol{\varepsilon} = \nabla^s \boldsymbol{u}_g$ (the subscript g in $\boldsymbol{u}_g$ indicates that this concerns a gradient-enriched displacement field). The equilibrium equations thus read

$$\nabla \cdot \Big(\boldsymbol{C} : \left(\nabla^s \boldsymbol{u}_g - \ell^2 \nabla^2 \nabla^s \boldsymbol{u}_g \right) \Big) + \boldsymbol{b} = \boldsymbol{0} \tag{2}$$

where $\boldsymbol{b}$ are the body forces.

2.1. The Ru-Aifantis operator split for elasticity

Equation (2) is a fourth-order differential equation in terms of the displacements, and its finite element implementation would therefore require $\mathcal{C}^1$-continuity of the shape functions. However, a simplification of Equation (2) is possible as shown by Ru and Aifantis (1993). An operator split can be applied such that Equation (2) is rewritten as

$$\nabla \cdot (\boldsymbol{C} : \nabla^s \boldsymbol{u}_c) + \boldsymbol{b} = \boldsymbol{0} \tag{3}$$

from which $\boldsymbol{u}_c$ can be computed. Afterwards, $\boldsymbol{u}_c$ serves as input for a second equation,

$$\boldsymbol{u}_g - \ell^2 \nabla^2 \boldsymbol{u}_g = \boldsymbol{u}_c \tag{4}$$

from which $\boldsymbol{u}_g$ is determined. Note that Equation (3) represents the equilibrium equations of classical elasticity. Therefore, $\boldsymbol{u}_c$ is interpreted as the displacements of classical elasticity. Instead of solving the fourth-order differential equations of expression (2), one must solve two sets of second-order differential equations.

The first of these is no different from classical elasticity and uses exactly the same boundary conditions, namely

$$\begin{aligned} \nabla \cdot \boldsymbol{\sigma} + \boldsymbol{b} = &\quad \mathbf{0} \qquad \text{in}\,\Omega, \\ \boldsymbol{\sigma}\boldsymbol{n} = &\quad \bar{\boldsymbol{t}} \qquad \text{on}\,\Gamma_t, \\ \boldsymbol{u}_c = &\quad \bar{\boldsymbol{u}} \qquad \text{on}\,\Gamma_u, \end{aligned} \tag{5}$$

where $\boldsymbol{n}$ is the outward unit normal to the boundary, $\bar{\boldsymbol{t}}$ are prescribed tractions on Γ_t and $\bar{\boldsymbol{u}}$ are prescribed displacements on Γ_u.

The second of these two equations, Equation (4), introduces the gradient effects and is accompanied by the following boundary conditions:

$$\left.\begin{aligned} &\boldsymbol{u}_g \cdot \boldsymbol{n} = \boldsymbol{u}_c \cdot \boldsymbol{n} \\ &\nabla(\boldsymbol{u}_g \cdot \boldsymbol{t}) \cdot \boldsymbol{n} = \nabla(\boldsymbol{u}_c \cdot \boldsymbol{t}) \cdot \boldsymbol{n} \end{aligned}\right\} \text{ on } \partial\Omega \tag{6}$$

where $\boldsymbol{n}$ and $\boldsymbol{t}$ are the directions normal and tangent to the boundary $\partial\Omega$ respectively.

As mentioned already, the gradient effects are absent in Equation (3), but gradient enriched displacements and, via derivation, strains can be obtained from Equation (4). Singularities are removed from these gradient-enriched strains (Askes et al., 2008), but not from the stresses since these are the same as in classical elasticity (Ru and Aifantis, 1993). The gradient-enriched strains can be subsequently used in the formulation of nonlinear material models, as explained in the next Section. Splitting the original fourth-order equation (2) into two second-order equations (3) and (4) has a major advantage for finite element applications, in that the widely available $\mathcal{C}^0$-continuous elements can be used, as has been explored by Tenek and Aifantis (2002) and Askes et al. (2008). Due to the specific uncoupled nature of this case, the two sets can be solved *sequentially*: firstly the classical local displacements $\boldsymbol{u}_c$ are resolved from Equation (3), after which they are used as a source term in Equation (4) so as to solve for $\boldsymbol{u}_g$.

2.2. Extension to inelasticity

To move from elasticity into inelasticity, the counterpart of Equation (3) is needed. A general framework is

$$\nabla \cdot \boldsymbol{\sigma}(\boldsymbol{\varepsilon}_a, \boldsymbol{\varepsilon}_g) + \boldsymbol{b} = \mathbf{0} \tag{7}$$

with the stress defined as

$$\boldsymbol{\sigma}(\boldsymbol{\varepsilon}_a, \boldsymbol{\varepsilon}_g) = \boldsymbol{C} : \boldsymbol{\varepsilon}_a - \boldsymbol{s}^{\text{inel}}(\boldsymbol{\varepsilon}_a, \boldsymbol{\varepsilon}_g) \tag{8}$$

where $\boldsymbol{\varepsilon}_g = \nabla^s \boldsymbol{u}_g$ is the gradient-enriched strain and $\boldsymbol{\varepsilon}_a = \nabla^s \boldsymbol{u}_a$ is the strain associated to the auxiliary displacement field $\boldsymbol{u}_a$ defined, in analogy with Equation (4), as

$$\boldsymbol{u}_g - \ell^2 \nabla^2 \boldsymbol{u}_g = \boldsymbol{u}_a \tag{9}$$

There are two important differences with the elastic case of Equations (3)–(4). Firstly, since $\boldsymbol{u}_a$ and $\boldsymbol{u}_g$ appear in both Equations (9) and (7), the system of equations is fully coupled: it is not possible to solve the equilibrium equation (7) for $\boldsymbol{u}_a$ and then use it as a source term in Equation (9) to compute $\boldsymbol{u}_g$. The second, closely related difference is that the auxiliary displacements $\boldsymbol{u}_a$ are *not* the classical displacements of local inelasticity. Nevertheless, in analogy to Bennett et al. (2007), $\boldsymbol{u}_a$ can be identified as the microscopic displacements whereas $\boldsymbol{u}_g$ are the macroscopic displacements. With this interpretation in mind, $\boldsymbol{u}_a$ are regarded as auxiliary local (i.e. unsmoothed) displacements in the remainder of this paper.

Note that the elastic part of the stress –that is, the first term in the RHS of Equation (8)– depends only on the local strain $\boldsymbol{\varepsilon}_a$, so the non-local strain $\boldsymbol{\varepsilon}_g$ only appears in the inelastic part of the stress, $\boldsymbol{s}^{\text{inel}}$. This choice is common in non-local models for damage and plasticity, see Bažant and Jirásek (2002). In addition, as shown in Section 3, it is the only format that regularises softening.

The general framework of Equation (8) was illustrated for damage models by Rodríguez-Ferran et al. (2004, 2005). Here it is extended to plasticity models, to illustrate its generality.

2.2.1. Damage model.

For non-local damage models, Equation (8) takes the form (Rodríguez-Ferran et al., 2004, 2005)

$$\boldsymbol{\sigma}(\boldsymbol{\varepsilon}_a, \boldsymbol{\varepsilon}_g) = [(1 - \omega(\boldsymbol{\varepsilon}_g)]\, \boldsymbol{C} : \boldsymbol{\varepsilon}_a \tag{10}$$

where ω is the damage parameter, driven by the non-local strain $\boldsymbol{\varepsilon}_g$. The inelastic stress is defined as

$$\boldsymbol{s}^{\text{inel}} = \omega(\boldsymbol{\varepsilon}_g) \boldsymbol{C} : \boldsymbol{\varepsilon}_a \tag{11}$$

The damage parameter ω depends on the non-local strain $\boldsymbol{\varepsilon}_g$ via the history variable κ, defined as

$$\kappa(t) = \max_{\tau \leq t} Y(t) \tag{12}$$

where Y is a scalar state variable. In a one-dimensional setting, Y is simply the scalar strain ε_g. In a multi-dimensional setting, Y is defined either as

$$Y = \sqrt{\sum_i \max(0, \varepsilon_i)^2} \tag{13}$$

where ε_i are the principal strains of $\boldsymbol{\varepsilon}_g$ (Mazars model, see Mazars (1986)) or as

$$Y = \frac{k-1}{2k(1-2\nu)} I_1 + \frac{1}{2k} \sqrt{\left(\frac{k-1}{1-2\nu} I_1 \right)^2 + \frac{12k}{(1+\nu)^2} J_2} \tag{14}$$

where $I_1 = \varepsilon_1 + \varepsilon_2 + \varepsilon_3$ and $J_2 = \frac{1}{6}\left[(\varepsilon_1 - \varepsilon_2)^2 + (\varepsilon_2 - \varepsilon_3)^2 + (\varepsilon_3 - \varepsilon_1)^2\right]$ are the first invariant and the second deviatoric invariant respectively (ε_i are the principal strains of $\boldsymbol{\varepsilon}_g$), ν the Poisson's ratio and k the ratio of compressive to tensile strength (modified von Mises criterion, see de Vree et al. (1995)).

Two different damage evolution laws are used: linear and exponential. The linear law is

$$\omega(\kappa) = \begin{cases} 0 & \text{if } \kappa \leq \kappa_i \\ \frac{\kappa_u(\kappa - \kappa_i)}{\kappa(\kappa_u - \kappa_i)} & \text{if } \kappa_i \leq \kappa \leq \kappa_u \\ 1 & \text{if } \kappa \geq \kappa_u \end{cases} \tag{15}$$

where κ_i is the damage initiation strain and κ_u is the ultimate strain. Equation (15) results in a linear softening branch in the stress-strain diagram. The constant slope of this branch facilitates the localisation analysis of the model, see Section 3.

The exponential law is

$$\omega = 1 - \frac{\kappa_i}{\kappa} \exp\big(-\beta(\kappa - \kappa_i) \big) \quad \text{for} \quad \kappa > \kappa_i \tag{16}$$

where κ_i is the damage initiation strain and β is a material parameter that controls the slope of the softening branch. This model is suitable for quasi-brittle materials such as concrete.

2.2.2. Plastic model with non-local plastic strain.

Several non-local models for softening plasticity can be found in the literature, and have been thoroughly analysed and compared in Jirásek and Rolshoven (2003) (integral-type models) and more recently in Jirásek and Rolshoven (2009a,b) (gradient models). These models can be accommodated in the general framework presented here.

Consider, as a first example, the model based on non-local plastic strain Bažant and Lin (1988):

$$\boldsymbol{\sigma}(\boldsymbol{\varepsilon}_a, \boldsymbol{\varepsilon}_g) = \boldsymbol{C} : (\boldsymbol{\varepsilon}_a - \boldsymbol{\varepsilon}_g^p) \tag{17}$$

In a displacement-based setting, the non-local plastic strain $\boldsymbol{\varepsilon}_g^p$ is obtained from an auxiliary *standard* plasticity model involving the non-local strain $\boldsymbol{\varepsilon}_g$ and a non-local stress $\boldsymbol{s}$ (different from stress $\boldsymbol{\sigma}$). This model reads

$$\begin{aligned}
&\text{Hooke's law} && \boldsymbol{s} = \boldsymbol{C} : (\boldsymbol{\varepsilon}_g - \boldsymbol{\varepsilon}_g^p) && (18)\\
&\text{Flow rule} && \dot{\boldsymbol{\varepsilon}}_g^p = \dot{\lambda}_g \boldsymbol{r}(\boldsymbol{s}, \boldsymbol{q}_g) && (19)\\
&\text{Softening rule} && \dot{\boldsymbol{q}}_g = -\dot{\lambda}_g \boldsymbol{h}(\boldsymbol{s}, \boldsymbol{q}_g) && (20)\\
&\text{Kuhn-Tucker conditions} && \dot{\lambda}_g \geq 0\,;\; f(\boldsymbol{s}, \boldsymbol{q}_g) \leq 0\,;\; \dot{\lambda}_g f(\boldsymbol{s}, \boldsymbol{q}_g) = 0 && (21)\\
&\text{Plastic consistency} && \dot{\lambda}_g \dot{f}(\boldsymbol{s}, \boldsymbol{q}_g) = 0 && (22)
\end{aligned}$$

Standard notation and concepts (see e.g. Simo and Hughes (1998)) are used in Equations (18)–(22). Equation (18) reflects the additive decomposition of strains into elastic and plastic strains. Plastic flow is governed by a generic flow rule $\boldsymbol{r}$ in Equation (19). The evolution of the internal variables $\boldsymbol{q}_g$ is described by a generic hardening/softening rule $\boldsymbol{h}$ in Equation (20). The yield function f and the plastic multiplier λ_g evolve according to the loading-unloading (or Kuhn-Tucker) conditions (21) and the consequent consistency (or persistency) condition (22), which establishes that the stress state should "persist" on the yield surface for plastic flow to occur. Note that the inelastic stress $\boldsymbol{s}^{\text{inel}} = \boldsymbol{C} : \boldsymbol{\varepsilon}_g^p$ only depends on the non-local strain.

The plastic model (18)-(22) is formally standard, in the sense that it involves only one (not two) strain fields and it is completely local (all non-local information already embedded into $\boldsymbol{\varepsilon}_g$). For this reason, the usual return mapping algorithms can be applied.

2.2.3. Plastic model with combination of local and non-local softening variables.

As discussed in Jirásek and Rolshoven (2003) and illustrated in Section 5.1 with a uniaxial tensile test, the plastic model based on non-local plastic strain locks for the late stages of softening. One possible remedy is to incorporate non-locality into the model via a weighted combination of local and non-local softening variables in the yield condition Vermeer and Brinkgreve (1994). This model reads

$$\text{Hooke's law} \qquad \boldsymbol{\sigma} = \boldsymbol{C} : (\boldsymbol{\varepsilon}_a - \boldsymbol{\varepsilon}_a^p) \tag{23}$$

$$\text{Flow rule} \qquad \dot{\boldsymbol{\varepsilon}}_a^p = \dot{\lambda}_a \boldsymbol{r}(\boldsymbol{\sigma}, \boldsymbol{q}_a) \tag{24}$$

$$\text{Softening rule} \qquad \dot{\boldsymbol{q}}_a = -\dot{\lambda}_a \boldsymbol{h}(\boldsymbol{\sigma}, \boldsymbol{q}_a) \tag{25}$$

$$\text{Kuhn-Tucker conditions} \qquad \dot{\lambda}_a \geq 0\,;\; f(\boldsymbol{\sigma}, \bar{\boldsymbol{q}}) \leq 0\,;\; \dot{\lambda}_a f(\boldsymbol{\sigma}, \bar{\boldsymbol{q}}) = 0 \tag{26}$$

$$\text{Weighted softening variable} \qquad \bar{\boldsymbol{q}} = (1-m)\boldsymbol{q}_a + m\boldsymbol{q}_g \tag{27}$$

$$\text{Plastic consistency} \qquad \dot{\lambda}_a \dot{f}(\boldsymbol{\sigma}, \bar{\boldsymbol{q}}) = 0 \tag{28}$$

Note that the softening variable $\bar{\boldsymbol{q}}$ is obtained from the local variable $\boldsymbol{q}_a$ and the non-local variable $\boldsymbol{q}_g$ (with weights $(1-m)$ and m), so the plastic model (23)-(28) must be solved in conjunction with the auxiliary model (18)-(22). This renders the model based on a combined local/non-local softening variable, which does not suffer from locking, more computationally demanding that the model based on non-local plastic strain.

2.3. Boundary conditions

Boundary conditions for the regularisation equation are a key ingredient in gradient-enriched formulations. For the displacement-based approach considered here, a natural choice is to prescribe non-homogeneous Dirichlet boundary conditions (Rodríguez-Ferran et al., 2004, 2005):

$$\boldsymbol{u}_g = \boldsymbol{u}_a \text{ on } \partial\Omega \tag{29}$$

Equation (29) has a clear physical meaning: auxiliary local and gradient non-local displacements coincide along the boundary. However, as noted in Jirásek and Marfia (2006), this can have the negative effect of not allowing displacement smoothing along the boundary. Such effect is especially detrimental in problems where localisation starts at the boundary (e.g. notched specimens).

To remedy this deficiency, non-homogeneous Neumann boundary conditions were proposed in Jirásek and Marfia (2006):

$$\nabla \boldsymbol{u}_g \cdot \boldsymbol{n} = \nabla \boldsymbol{u}_a \cdot \boldsymbol{n} \text{ on } \partial\Omega \tag{30}$$

($\boldsymbol{n}$ is the outward unit normal). Equation (30) permits displacement smoothing along the boundary, because $\boldsymbol{u}_g$ and $\boldsymbol{u}_a$ may be different on $\partial\Omega$. However, it does not ensure volume preservation. Assuming a constant density, this condition reads

$$0 = \int_\Omega \nabla \cdot (\boldsymbol{u}_g - \boldsymbol{u}_a) d\Omega = \int_{\partial\Omega} (\boldsymbol{u}_g - \boldsymbol{u}_a) \cdot \boldsymbol{n} \, d\Gamma \tag{31}$$

where the divergence theorem has been applied. Equation (31) and the above discussion suggest the following combined boundary conditions:

$$\left.\begin{array}{l} \boldsymbol{u}_g \cdot \boldsymbol{n} = \boldsymbol{u}_a \cdot \boldsymbol{n} \\ \nabla(\boldsymbol{u}_g \cdot \boldsymbol{t}) \cdot \boldsymbol{n} = \nabla(\boldsymbol{u}_a \cdot \boldsymbol{t}) \cdot \boldsymbol{n} \end{array}\right\} \text{ on } \partial\Omega \tag{32}$$

The essential boundary condition $(32)_1$ ensures volume preservation, whereas the natural boundary condition $(32)_2$ allows displacement smoothing along the tangent $\boldsymbol{t}$ to the boundary. It may be argued that volume preservation is not essential, because $\boldsymbol{u}_g$ is simply an auxiliary displacement field used to regularise the problem. However, volume preservation has a clear geometrical meaning and does not preclude smoothing along the boundary, as shown above. These combined boundary conditions have been used in the two-dimensional examples of Section 5. Note that, in a one-dimensional setting, Equation (32) reduces to the Dirichlet boundary conditions (29).

3. LOCALISATION ANALYSIS

A localisation analysis is carried out with a twofold aim: (i) investigate appropriate formats of the constitutive equations for damage and plasticity, and (ii) establish expressions for the critical wave length that can be used to estimate a priori the width of the localisation zone. The one-dimensional governing equations are written as

$$0 = \sigma'(\varepsilon_a, \varepsilon_g) = \frac{\partial \sigma}{\partial \varepsilon_a} u_a'' + \frac{\partial \sigma}{\partial \varepsilon_g} u_g'' \tag{33}$$

where a superimposed comma denotes an x-derivative. Equation (33) is used together with

$$u_a = u_g - \ell^2 u_g'' \tag{34}$$

A uniform reference state ε_0 is assumed, and infinitesimal perturbations are taken as $u_a = u_0 + \delta u_a$ together with $u_g = u_0 + \delta u_g$. Note that the reference displacement u_0 is linear and results in a uniform strain $\varepsilon_a = \varepsilon_g = \varepsilon_0$. The perturbations are taken as general harmonic functions through $\delta u_a = A_1 \cos kx$ and $\delta u_g = A_2 \cos kx$, where k is the wave number and the two amplitudes are denoted A_1 and A_2. We require strain fields that are regularised yet allow for strain concentrations; hence, k should be finite and real, If k is not finite and real, the solution may be non-regularised (leading to Dirac-delta type strain fields) or over regularised (precluding any localisation of strain), but examining the exact nature of such cases is beyond the scope of our study.

A relation between these two amplitudes is found by substituting the two perturbation into Equation (34), which yields

$$A_1 = A_2 \left(1 + k^2 \ell^2\right) \tag{35}$$

Similarly, substituting the two perturbations into Equation (33) renders

$$A_1 \frac{\partial \sigma}{\partial \varepsilon_a} + A_2 \frac{\partial \sigma}{\partial \varepsilon_g} = 0 \tag{36}$$

Finally, substituting Equation (35) into Equation (36) gives

$$\frac{\partial \sigma}{\partial \varepsilon_a} + \frac{\partial \sigma}{\partial \varepsilon_g} \frac{1}{1 + k^2 \ell^2} = 0 \tag{37}$$

3.1. Damage model

For uniaxial tension, $\kappa \equiv Y \equiv \varepsilon$, and the damage loading function is given by

$$\omega(\varepsilon) = \frac{\kappa_u(\varepsilon - \kappa_i)}{\varepsilon(\kappa_u - \kappa_i)} \qquad \text{by which} \qquad \frac{\partial \omega}{\partial \varepsilon} = \frac{\kappa_i \kappa_u}{\varepsilon^2(\kappa_u - \kappa_i)} \tag{38}$$

Four different formats of the constitutive law will be distinguished, depending on which strain (ε_a or ε_g) is used.

format 1: It is assumed that $\sigma = (1 - \omega(\varepsilon_a))E\varepsilon_a$. When this is substituted into Equation (37), one obtains

$$\frac{\kappa_i E}{\kappa_u - \kappa_i} = 0 \tag{39}$$

which does not depend on k and has no solution. This format is not suitable for regularisation.

format 2: The stress-strain relation is taken as $\sigma = (1 - \omega(\varepsilon_a))E\varepsilon_g$. Substitution into Equation (37) gives

$$\frac{\kappa_i E}{\kappa_u - \kappa_i}\left(1 + \frac{\kappa_u}{\varepsilon_0}k^2\ell^2\right) = 0 \tag{40}$$

which again leads to an imaginary wave number k (i.e. model not regularised).

format 3: Next, it is assumed that $\sigma = (1 - \omega(\varepsilon_g))E\varepsilon_a$. This is combined with Equation (37) and yields

$$\frac{\kappa_i E}{\kappa_u - \kappa_i}\left[-1 + \left(\frac{\kappa_u}{\varepsilon_0} - 1\right)k^2\ell^2\right] = 0 \tag{41}$$

resulting in a real wave number k_{crit}, which means that this format is suitable for regularisation.

format 4: Finally, $\sigma = (1 - \omega(\varepsilon_g))E\varepsilon_g$ is investigated. Equation (37) can then be elaborated as

$$\frac{\kappa_i E}{\kappa_u - \kappa_i}\frac{1}{1 + k^2\ell^2} = 0 \tag{42}$$

which leads to an infinite wave number k (i.e. format not suitable for regularisation).

3.2. Plasticity model with non-local plastic strain

Similar to damage, a piecewise linear stress-strain relation is assumed. The one-dimensional model can be written as

$$\dot{\sigma} = E\dot{\varepsilon} - \dot{s}^{\text{inel}}(\dot{\varepsilon}) \qquad \text{in which} \qquad \dot{s}^{\text{inel}}(\dot{\varepsilon}) = \frac{E^2}{E + H}\,\dot{\varepsilon} \tag{43}$$

where H is the hardening modulus. Again, four different formats of the constitutive law are studied.

format 1: The stress-strain relation is taken as $\dot{\sigma} = E\dot{\varepsilon}_a - \dot{s}^{\text{inel}}(\dot{\varepsilon}_a)$. Substitution into Equation (37) yields

$$\frac{EH}{E+H} = 0 \tag{44}$$

This format is not valid for regularisation.

format 2: Next, it is assumed that $\dot{\sigma} = E\dot{\varepsilon}_g - \dot{s}^{\text{inel}}(\dot{\varepsilon}_a)$. Combined with Equation (37) this gives

$$\frac{EH}{E+H}\left(1 - \frac{E}{H}k^2\ell^2\right) = 0 \tag{45}$$

For softening ($H < 0$), this leads to an imaginary wave number.

format 3: With an assumed stress-strain relation as $\dot{\sigma} = E\dot{\varepsilon}_a - \dot{s}^{\text{inel}}(\dot{\varepsilon}_g)$, Equation (37) yields

$$\frac{EH}{E+H}\left(1 + \frac{E+H}{H}k^2\ell^2\right) = 0 \tag{46}$$

A real wave number k_{crit} is obtained for negative H under the condition that $E + H > 0$. This format is valid for regularisation.

format 4: Finally, $\dot{\sigma} = E\dot{\varepsilon}_g - \dot{s}^{\text{inel}}(\dot{\varepsilon}_g)$ is tested. When this is substituted into Equation (37), the result is

$$\frac{EH}{E+H}\frac{1}{1+k^2\ell^2} = 0 \tag{47}$$

which leads to an infinite wave number k. Thus, this format is not good for regularisation.

The above localisation analysis shows that, for both models, the only combination of strains that regularises softening is format 3 (i.e. strain ε_a in the elastic part of the stress, and softening driven by ε_g). Of course, format 1 (local model with no enrichment) has no regularisation capabilities. The analysis also shows that format 4 (i.e. "fully" enriched model) and format 2 (inverse of format 3) are invalid combinations as well. This is in correspondence with the numerical results of Chang et al. (2002) for damage with format 3.

3.3. Plasticity model with local/non-local softening variable

The non-locking plasticity model is considered now. The goal is to assess the influence of the weighting parameter m on its regularisation capabilities.

The one-dimensional model can be written as

$$\dot{\sigma} = \frac{EH(1-m)}{E+H(1-m)}\dot{\varepsilon}_a + \frac{E^2Hm}{(E+H)[E+H(1-m)]}\dot{\varepsilon}_g \tag{48}$$

Substitution into Equation (37) renders

$$\frac{EH(1-m)}{E+H(1-m)} + \frac{E^2Hm}{(E+H)[E+H(1-m)]}\frac{1}{1+k^2\ell^2} = 0 \tag{49}$$

As a first check, note that Equation (49) coincides with Equation (44) if $m = 0$ and with Equation (47) if $m = 1$. These are the expected results, because the model is local for $m = 0$ and "fully" enriched for $m = 1$.

Equation (49) can be recast as

$$\frac{EH}{E+H(1-m)}\left[1 + m\left(\frac{E}{E+H}\frac{1}{1+k^2\ell^2} - 1\right)\right] = 0 \tag{50}$$

which has a real solution k_{crit} if $m > 1$ or $m < 1 + E/H$. It is interesting to note that the requirement $m > 1$ is common to all the versions of the model: the one based on two displacement fields presented here, and the original ones based on regularising the softening variable, either with an integral-type approach (Jirásek and Rolshoven, 2003) or with a gradient approach (Jirásek and Rolshoven, 2009b).

Although a (large) negative $m < 1 + E/H$ is admissible according to Equation (50), it does not render a regularised model. In fact, as shown by Jirásek and Rolshoven (2009b), a positive "local" plastic modulus $(1-m)H$ is needed (that is, $m > 1$).

3.4. Critical wave lengths

The width of the zone in which strain localisation is active can be estimated from the critical wave length λ_{crit} associated to the critical wave number k_{crit}. For the damage formulation (format 3) it is found that

$$k_{\text{crit}} = \frac{1}{\ell}\sqrt{\frac{\varepsilon_0}{\kappa_u - \varepsilon_0}} \quad ; \quad \lambda_{\text{crit}} = \frac{2\pi}{k_{\text{crit}}} = 2\pi\ell\sqrt{\frac{\kappa_u - \varepsilon_0}{\varepsilon_0}} \tag{51}$$

For the plasticity model with non-local plastic strain (again format 3) one obtains

$$k_{\text{crit}} = \frac{1}{\ell}\sqrt{\frac{-H}{E+H}} \quad ; \quad \lambda_{\text{crit}} = \frac{2\pi}{k_{\text{crit}}} = 2\pi\ell\sqrt{\frac{E+H}{-H}} \tag{52}$$

Finally, for the plasticity model with weighted local/non-local softening variable, the critical wave length is

$$\lambda_{\text{crit}} = \frac{2\pi}{k_{\text{crit}}} = 2\pi\ell\sqrt{\frac{(1-m)(E+H)}{-E-H(1-m)}} \tag{53}$$

so, for the value $m = 2$ suggested by Jirásek and Rolshoven (2003), one gets

$$\lambda_{\text{crit}} = \frac{2\pi}{k_{\text{crit}}} = 2\pi\ell\sqrt{\frac{E+H}{E-H}} \tag{54}$$

4. FINITE ELEMENT DISCRETISATION

The derivation of the weak form of Equations (7) and (9) and its finite element discretisation are standard, and leads to

$$\mathbf{r}_{\text{equil}}(\mathbf{u}_a, \mathbf{u}_g) := \mathbf{f}_{\text{int}}(\mathbf{u}_a, \mathbf{u}_g) - \mathbf{f}_{\text{ext}} = \mathbf{0} \tag{55}$$

$$\mathbf{r}_{\text{regu}}(\mathbf{u}_a, \mathbf{u}_g) := -\mathbf{M}\mathbf{u}_a + (\mathbf{M} + \ell^2\mathbf{D})\mathbf{u}_g = \mathbf{0} \tag{56}$$

Note that upright boldface is used for finite element vectors and matrices: the nodal displacements $\mathbf{u}_a$ and $\mathbf{u}_g$; the internal and external forces $\mathbf{f}_{\text{int}}$ and $\mathbf{f}_{\text{ext}}$; the (non-linear) equilibrium residual $\mathbf{r}_{\text{equil}}(\mathbf{u}_a, \mathbf{u}_g)$ and the (linear) regularisation residual $\mathbf{r}_{\text{regu}}(\mathbf{u}_a, \mathbf{u}_g)$; and the mass and diffusivity matrices, defined as

$$\mathbf{M} = \int_\Omega \mathbf{N}^T\mathbf{N}d\Omega \quad \text{and} \quad \mathbf{D} = \int_\Omega \nabla\mathbf{N}^T\nabla\mathbf{N}d\Omega \tag{57}$$

with $\mathbf{N}$ the matrix of shape functions and $\nabla\mathbf{N}$ the matrix of shape function gradients. The Voigt notation is used, so $\boldsymbol{\sigma}$, $\boldsymbol{\varepsilon}_a$ and $\boldsymbol{\varepsilon}_g$ now represent the usual finite element vectors rather than tensors. The internal force vector is defined as

$$\mathbf{f}_{\text{int}} = \int_\Omega \mathbf{B}^T\boldsymbol{\sigma}(\boldsymbol{\varepsilon}_a, \boldsymbol{\varepsilon}_g)d\Omega \tag{58}$$

where $\mathbf{B}$ is the usual matrix of shape function derivatives. The integrals in Equations (57) and (58) are typically approximated by means of a Gaussian quadrature.

Consistent linearisation is required for the solution of Equations (55) and (56) by means of Newton's method, and results in

$$\begin{bmatrix} \mathbf{K}_{aa}^i & \mathbf{K}_{ag}^i \\ -\mathbf{M} & (\mathbf{M}+\ell^2\mathbf{D}) \end{bmatrix} \begin{Bmatrix} \delta\mathbf{u}_a^{i+1} \\ \delta\mathbf{u}_g^{i+1} \end{Bmatrix} = \begin{Bmatrix} -\mathbf{r}_{\text{equil}}^i \\ \mathbf{0} \end{Bmatrix} \tag{59}$$

where i is the iteration counter, $\delta\mathbf{u}$ is the iterative correction in displacements, and the stiffness matrices are

$$\mathbf{K}_{aa} := \frac{\partial \mathbf{r}_{\text{equil}}}{\partial \mathbf{u}_a} = \int_\Omega \mathbf{B}^T \frac{\partial \Delta\boldsymbol{\sigma}(\boldsymbol{\varepsilon}_a, \boldsymbol{\varepsilon}_g)}{\partial \Delta\boldsymbol{\varepsilon}_a} \mathbf{B} d\Omega \tag{60}$$

$$\mathbf{K}_{ag} := \frac{\partial \mathbf{r}_{\text{equil}}}{\partial \mathbf{u}_g} = \int_\Omega \mathbf{B}^T \frac{\partial \Delta\boldsymbol{\sigma}(\boldsymbol{\varepsilon}_a, \boldsymbol{\varepsilon}_g)}{\partial \Delta\boldsymbol{\varepsilon}_g} \mathbf{B} d\Omega \tag{61}$$

where finite (rather than infinitesimal) increments of stress and strain are taken for consistency.

The computational efficiency of regularising the problem at the level of displacements is clear from Equation (59): since the residual $\mathbf{r}_{\text{regu}}$ is linear, the two blocks in the second row of Equation (59) are constant and $\mathbf{r}_{\text{regu}}^i$ is zero after the first iteration. This is not the case in standard gradient models, where the regularisation equation (written in terms of, say, inelastic strains or state variables) is nonlinear Rodríguez-Ferran et al. (2005).

4.1. Damage

For the damage model of Equation (10), the tangent operators are

$$\frac{\partial \Delta\boldsymbol{\sigma}(\boldsymbol{\varepsilon}_a, \boldsymbol{\varepsilon}_g)}{\partial \Delta\boldsymbol{\varepsilon}_a} = [(1-\omega(\boldsymbol{\varepsilon}_g)]\,\mathbf{C} \quad \text{and} \quad \frac{\partial \Delta\boldsymbol{\sigma}(\boldsymbol{\varepsilon}_a, \boldsymbol{\varepsilon}_g)}{\partial \Delta\boldsymbol{\varepsilon}_g} = -\mathbf{C}\boldsymbol{\varepsilon}_a \frac{\partial \omega}{\partial \boldsymbol{\varepsilon}_g} \tag{62}$$

so the stiffness matrices are

$$\mathbf{K}_{aa} = \int_\Omega \mathbf{B}^T\,[(1-\omega(\boldsymbol{\varepsilon}_g)]\,\mathbf{C}\mathbf{B} d\Omega \tag{63}$$

$$\mathbf{K}_{ag} = -\int_\Omega \mathbf{B}^T \mathbf{C}\boldsymbol{\varepsilon}_a \frac{\partial \omega}{\partial \boldsymbol{\varepsilon}_g} \mathbf{B} d\Omega \tag{64}$$

Note that $\mathbf{K}_{aa}$ in Equation (63) is the usual secant matrix, whereas $\mathbf{K}_{ag}$ is the tangent contribution to the stiffness. The only difference with respect to a local damage model is that this latter matrix depends on both strain fields.

4.2. Plasticity

Similarly, if the plastic model with non-local plastic strain is used, see Section 2.2.2, the tangent operators are

$$\frac{\partial \Delta\boldsymbol{\sigma}(\boldsymbol{\varepsilon}_a, \boldsymbol{\varepsilon}_g)}{\partial \Delta\boldsymbol{\varepsilon}_a} = \mathbf{C}_a \quad \text{and} \quad \frac{\partial \Delta\boldsymbol{\sigma}(\boldsymbol{\varepsilon}_a, \boldsymbol{\varepsilon}_g)}{\partial \Delta\boldsymbol{\varepsilon}_g} = \mathbf{C}_g \tag{65}$$

where

$$\mathbf{C}_a = \mathbf{C} \tag{66}$$

$$\mathbf{C}_g = \mathbf{C}_c^{\text{ep}} - \mathbf{C} \tag{67}$$

with

$$\mathbf{C}_c^{\text{ep}} = \mathbf{C}_c - \frac{(\mathbf{C}_c : \nabla_{\boldsymbol{s}} f)\,(\nabla_{\boldsymbol{s}} f : \mathbf{C}_c)}{H + \nabla_{\boldsymbol{s}} f : \mathbf{C}_c : \nabla_{\boldsymbol{s}} f} \tag{68}$$

$$\mathbf{C}_c = \left(\mathbf{C}^{-1} + \Delta\lambda_g : \nabla_{\boldsymbol{s}}^2 f\right)^{-1} \tag{69}$$

For simplicity, an associated flow rule $\boldsymbol{r} = \frac{\partial f}{\partial \boldsymbol{s}}$ and only one internal variable q_g are assumed. Note that Equations (68) and (69) are the standard definitions of the consistent tangent operators for the auxiliary model in terms of $\boldsymbol{s}$ and $\boldsymbol{\varepsilon}_g$.

For the plastic model with combined local/non-local softening variables, see Section 2.2.3, the tangent operators are

$$\mathbf{C}_a = \mathbf{C}_{c,a} - \frac{(\mathbf{C}_{c,a} : \nabla_{\boldsymbol{\sigma}} f_a)(\nabla_{\boldsymbol{\sigma}} f_a : \mathbf{C}_{c,a})}{(1-m)H + \nabla_{\boldsymbol{\sigma}} f_a : \mathbf{C}_{c,a} : \nabla_{\boldsymbol{\sigma}} f_a} \tag{70}$$

$$\mathbf{C}_g = \frac{mH(\mathbf{C}_{c,a} : \nabla_{\boldsymbol{\sigma}} f_a)(\nabla_{\boldsymbol{s}} f_g : \mathbf{C}_{c,g})}{[(1-m)H + \nabla_{\boldsymbol{\sigma}} f_a : \mathbf{C}_{c,a} : \nabla_{\boldsymbol{\sigma}} f_a]\,[H + \nabla_{\boldsymbol{s}} f_g : \mathbf{C}_{c,g} : \nabla_{\boldsymbol{s}} f_g]} \tag{71}$$

with $\mathbf{C}_{c,a}$ and $\mathbf{C}_{c,g}$ given by Equation (69).

The stiffness matrices are now

$$\mathbf{K}_{aa} = \int_\Omega \mathbf{B}^T \mathbf{C}_a \mathbf{B} d\Omega \tag{72}$$

$$\mathbf{K}_{ag} = \int_\Omega \mathbf{B}^T \mathbf{C}_g \mathbf{B} d\Omega \tag{73}$$

In this case, $\mathbf{K}_{aa}$ is simply the elastic stiffness matrix (so it does not depend on the iteration counter i) and $\mathbf{K}_{ag}$ is the tangent contribution. Again, the only difference with respect to a local model is that this latter matrix depends on the two strain fields rather than only local strains $\boldsymbol{\varepsilon}$.

5. NUMERICAL EXAMPLES

5.1. Uniaxial tensile test

The regularisation capabilities are assessed first by means of a uniaxial tensile test, see Figure 1 and Rodríguez-Ferran et al. (2005).

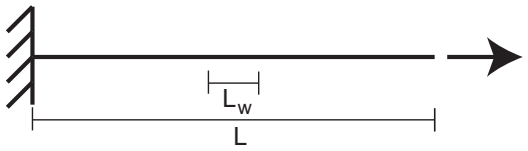

Figure 1: Uniaxial tensile test

The central tenth of the bar is weakened (10% reduction in Young's modulus) to trigger localisation. The geometrical and material parameters are summarised in Table 1. As suggested in Jirásek and Rolshoven (2003), the weighted softening variable of Equation (27) is computed with $m = 2$. The numerical tests are displacement-controlled. The three inelastic models (damage and two plasticity models) will be discussed in parallel.

Table 1: Uniaxial tensile test. Geometrical and material parameters

Meaning	**Symbol**	**Value**
Length of bar	L	100 cm
Idem of weakened part	L_W	10 cm
Cross-section of bar	A	1 cm^2
Young's modulus	E	20 000 MPa
Idem of weaker part	E_W	18 000 MPa
Damage model		
Damage threshold	κ_i	10^{-4}
Ultimate strain	κ_u	1.25×10^{-2}
Plasticity models		
Initial yield stress	σ_Y	2 MPa
Idem of weakened part	$\sigma_{Y,W}$	1.8 MPa
Softening modulus (Section 2.2.2)	H	−2000 MPa
Softening modulus (Section 2.2.3)	H	−200 MPa
Weighting parameter m (Section 2.2.3)	m	2

The goal of the first analysis is to check whether the models regularise softening. A fixed internal length $\ell = \sqrt{5}$ cm and five different meshes of 40,

80, 160, 320 and 640 elements (corresponding respectively to element sizes h of 2.5, 1.25, 0.625, 0.3125 and 0.15625 cm) are used.

The results are summarised in Figure 2. The excellent agreement in force-displacement curves of Figures 2(a), 2(c) and 2(e) clearly indicates that mesh dependency is completely removed. Indeed, as shown in Figures 2(b), 2(d) and 2(f), the width of the localisation band does not depend on the element size.

Figure 2 also shows the different response at the late stages of softening between the two plasticity models. The model based on non-local plastic strain locks and does not unload to zero stress, see Figure 2(c), and exhibits an expanding plastic strain profile, see Figure 2(d). The model based on a weighted local/non-local softening variable, on the other hand, is locking-free, see Figures 2(e) and 2(f).

In the second analysis, a fixed mesh of 80 elements and different values of the internal length ℓ (1, $\sqrt{2}$, $\sqrt{5}$, $\sqrt{10}$, $\sqrt{20}$ and $\sqrt{40}$ cm) are considered. The results are summarised in Figures 3 (damage model) and 4 (plastic model with local/non-local softening variable). Note that, as desired, both the ductility in the force-displacement response and the width of the localisation zone increase with the internal length.

In fact, the relation between the internal length scale and the width of the localisation zone is provided by the localisation analysis of Section 3. The critical wave lengths are $\lambda_{\text{crit}} = 2\pi\ell\sqrt{(\kappa_u - \kappa_i)/\kappa_i}$ for the damage model and $\lambda_{\text{crit}} = 2\pi\ell\sqrt{(E+H)/(E-H)}$ for the plasticity model with local/non-local softening variable, see Eqs. (51) and (54) where we have substituted $\varepsilon_0 = \kappa_i$ to evaluate the critical wave length at damage initiation.

The values of λ_{crit} and the width of the localisation zone for the different ℓ are shown in Table 2. The agreement is excellent for the damage model, see Figure 3(b). For the plastic model the relation is not so straight-forward, because two different plastic strains are involved. Table 2 shows, however, that the critical wave length is an intermediate value between the two possible definitions of "width of localisation zone", see Figures 4(b) and (c).

The expressions of the critical wave length in Section 3 also provide insight in the different qualitative behaviour of the two plasticity models. To avoid negative yield stresses, the softening modulus is set to zero when the yield stress is null. Setting $H = 0$ results in an infinite critical wave length for the model with non-local plastic strain, see Equation (52), so the width of the localisation zone expands. For the model with local/non-local softening

variable, on the other hand, the critical wave length remains finite for $H = 0$, see Equation (54), and so does the width of localisation.

Table 2: Uniaxial tensile test: critical wave length vs. observed width of localisation zone (in cm)

Damage model				
ℓ	1	$\sqrt{2}$	$\sqrt{5}$	$\sqrt{10}$
λ_{crit}	21.3	30.1	47.6	67.8
width in Figure 3(b)	22.5	30	50	77.5

Plasticity model with local/non-local softening variable					
ℓ	1	$\sqrt{5}$	$\sqrt{10}$	$\sqrt{20}$	$\sqrt{40}$
λ_{crit}	6.2	13.9	19.7	27.8	39.3
width in Figure 4(b)	5	10	15	20	27.5
width in Figure 4(c)	12.5	27.5	37.5	55	77.5

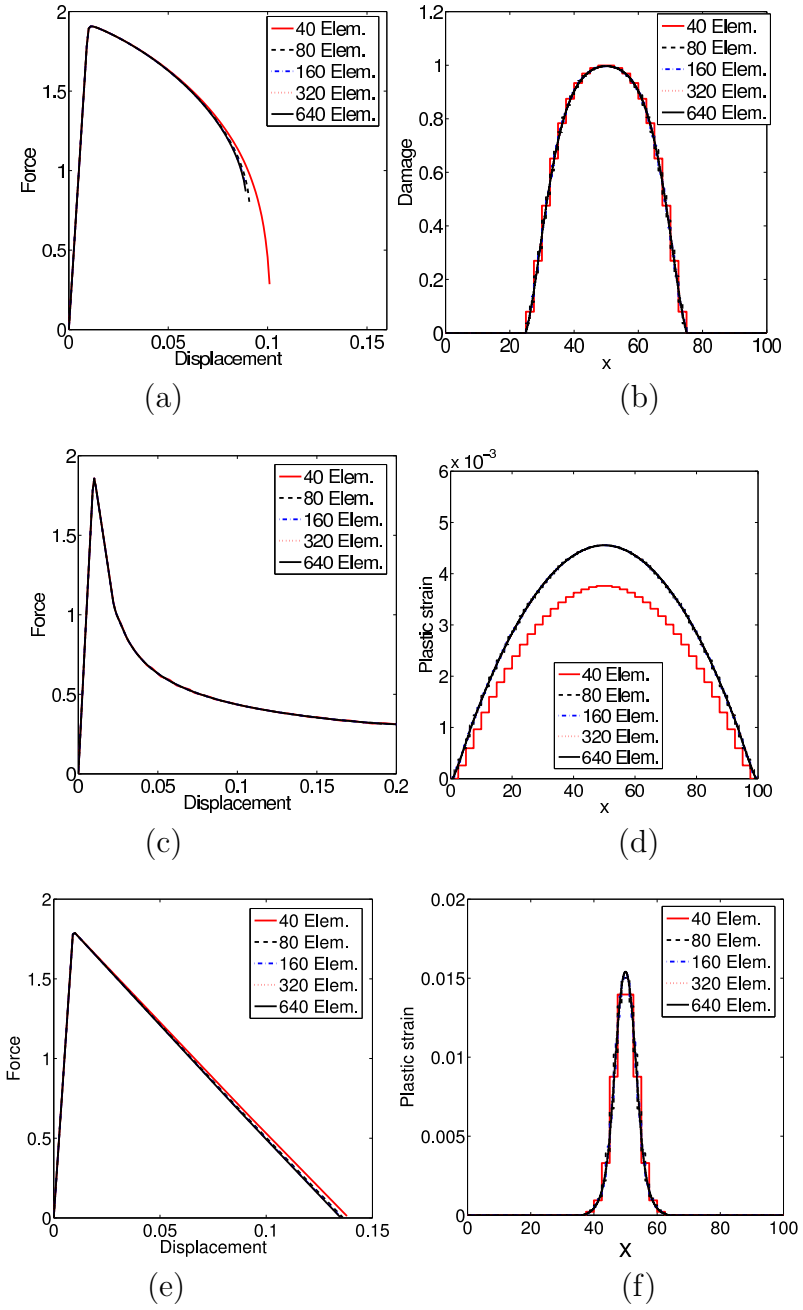

Figure 2: Influence of mesh size on uniaxial tensile test: force-displacement curves (left) and localisation zone (right) for damage model (top row), plasticity model with non-local plastic strain (middle row) and plasticity model with local/non-local softening variable (bottom row).

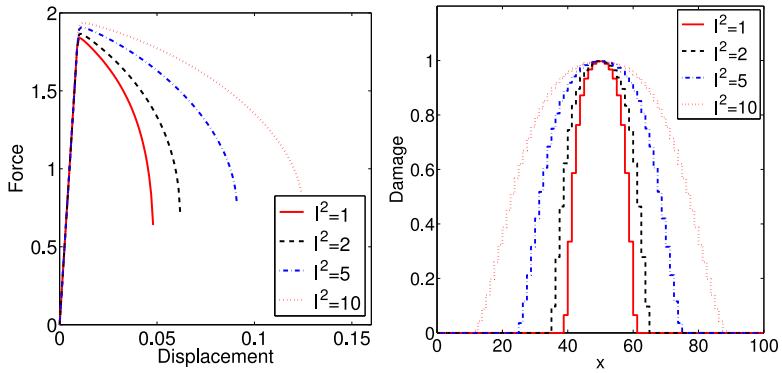

Figure 3: Influence of internal length ℓ on uniaxial tensile test – damage model: (a) force-displacement curves; (b) final profiles of damage ω.

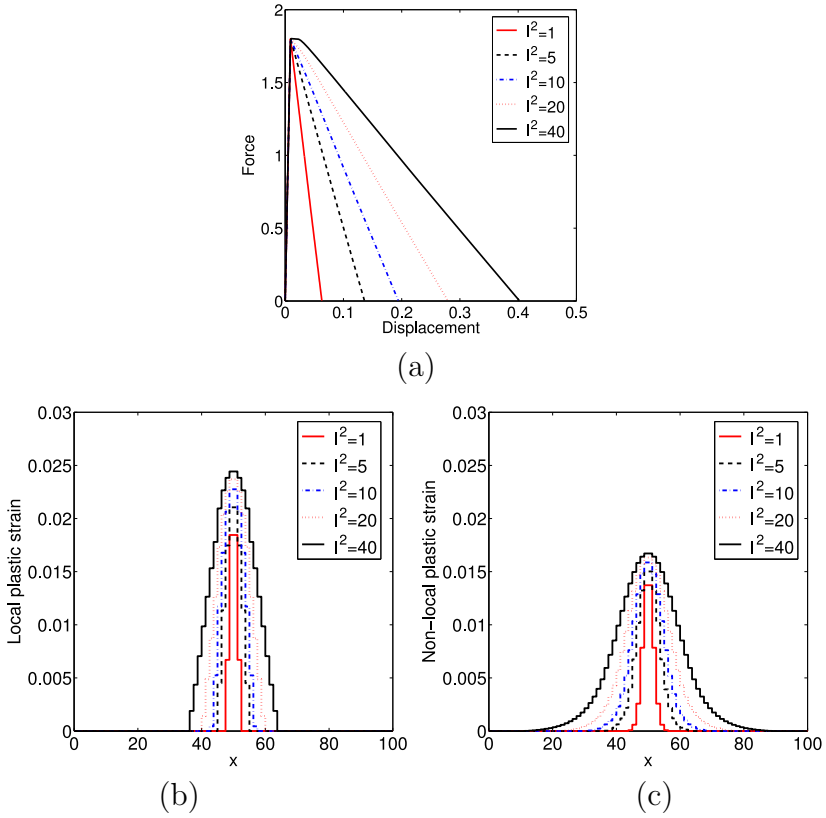

Figure 4: Influence of internal length ℓ on uniaxial tensile test – plastic model with weighted softening variable: (a) force-displacement curves; (b) final profiles of local plastic strain ε_a^p; (c) final profiles of non-local plastic strain ε_g^p.

5.2. Biaxial compression test

The classical biaxial compression test (Pamin, 1994; de Borst and Pamin, 1996) is analysed next using a von Mises plastic model with linear softening and non-local plastic strain, see Section 2.2.2. As in Pamin (1994), the case with an imperfection at the left bottom corner is used to illustrate mesh insensitivity, whereas the case with a centred imperfection illustrates imperfection size insensitivity. The material and geometrical parameters are summarised in Table 3.

Table 3: Biaxial compression test. Geometrical and material parameters

Meaning	**Symbol**	**Value**
Height of specimen	L	120 mm
Width of specimen	B	60 mm
Shear modulus	G	4000 MPa
Poisson's ratio	ν	0.3
Initial yield stress	σ_Y	100 MPa
Idem of imperfection	$\sigma_{Y,W}$	90 MPa
Softening modulus	H	-400 MPa
Internal length scale	ℓ	0.5 mm

Figure 5 shows the four finite element meshes used for the first analysis. Note that the bottom corner imperfection has a constant size of 10×10. The results are clearly mesh-insensitive in all the relevant outputs: deformation patterns, Figure 6(a); plastic strain profiles, Figure 6(b); force-displacement curves, Figure 7.

In the second analysis, the medium mesh of 12×24 elements and two centred imperfections of sizes 5×5 and 25×25 are used, see Figure 8. Again, mesh-insensitive results are obtained, see Figures 9 and 10.

To sum up: neither the finite element size nor the imperfection size control the mechanical response. This clearly shows the gradient-enriched plasticity model also regularises softening in a multidimensional setting.

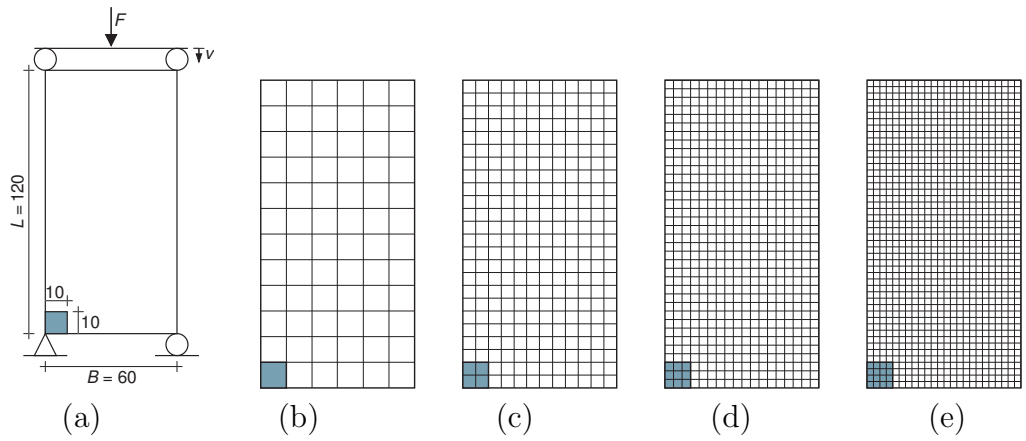

Figure 5: Biaxial compression test: (a) problem statement; finite element meshes of (b) 6×12 elements; (c) 12×24 elements; (d) 18×36 elements; (e) 24×48 elements

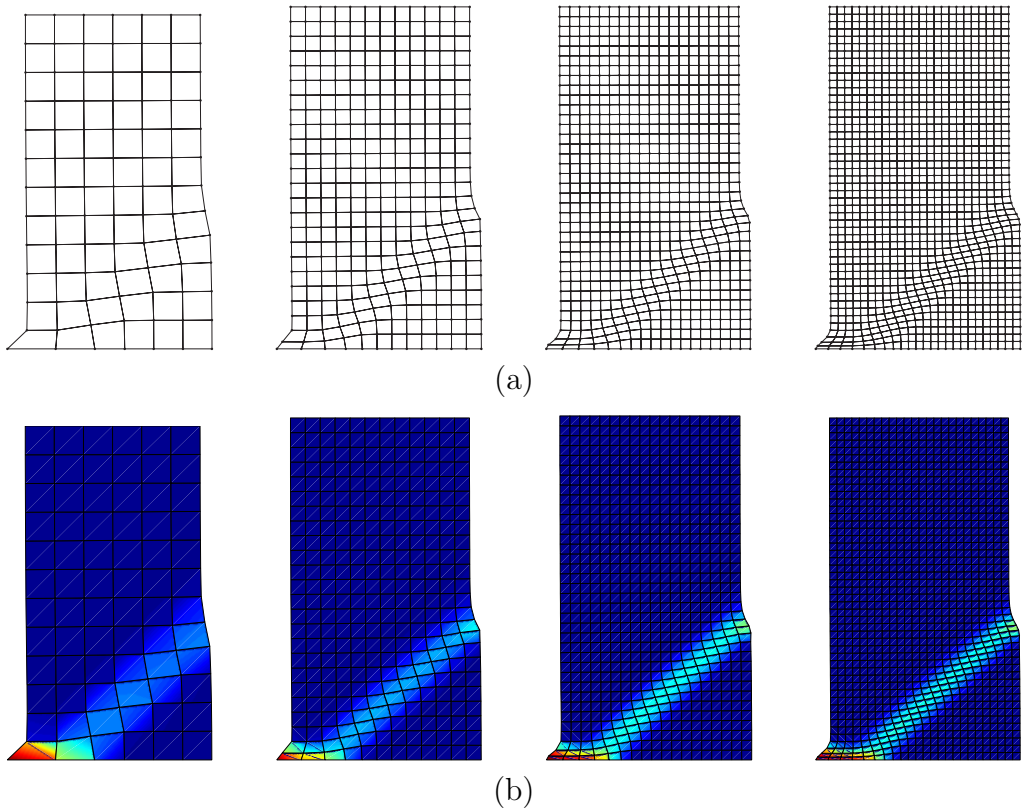

Figure 6: Biaxial compression test: (a) deformation pattern and (b) equivalent plastic strain for the four finite element meshes

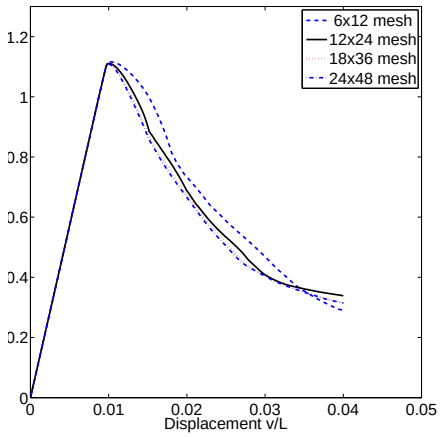

Figure 7: Biaxial compression test: force-displacement curves for the four finite element meshes

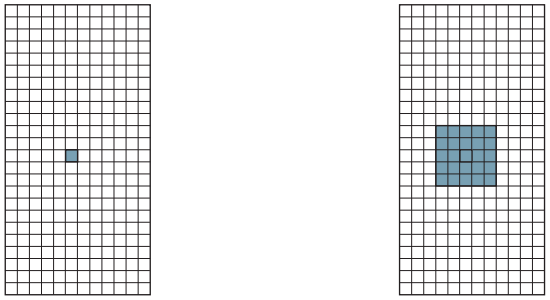

Figure 8: Biaxial compression test: (a) small imperfection; (b) large imperfection

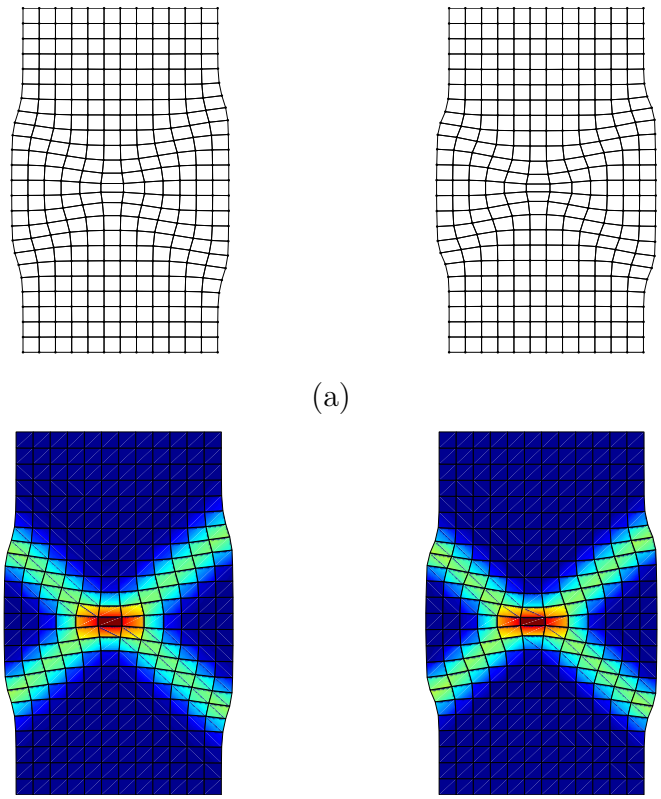

Figure 9: Biaxial compression test: (a) deformation patterns and (b) equivalent plastic strain for the two imperfection sizes

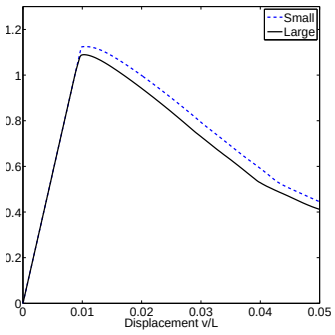

Figure 10: Biaxial compression test: force-displacement curves for the two imperfection sizes

5.3. Direct tension test

As a final example of softening regularisation, a direct tension test is simulated, see Figure 11(a). A square plate is clamped at the right edge and subjected to a linear distribution of displacements at the top and bottom edges. A damage model with the Mazars definition of the state variable and linear softening is used, see Section 2.2.1. An imperfection of constant length and variable width (one finite element) triggers localisation. The geometrical and material parameters are summarised in Table 4.

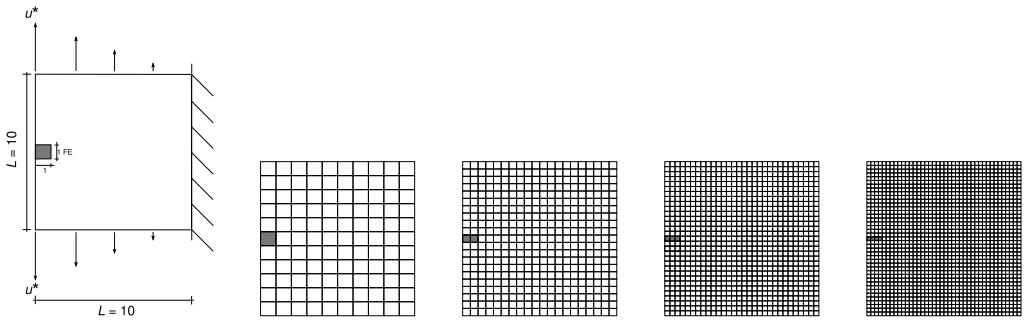

Figure 11: Direct tension test: (a) problem statement; finite element meshes of (b) 10×11 elements; (c) 20×21 elements; (d) 30×31 elements; (e) 40×41 elements

Table 4: Direct tension test. Geometrical and material parameters

Meaning	**Symbol**	**Value**
Size of specimen	L	10 cm
Length of weaker part	L_W	1 cm
Width of weaker part	h_W	1 finite element
Young's modulus	E	20 000 MPa
Idem of weaker part	E_W	2 000 MPa (90% reduction in E)
Damage threshold	κ_i	10^{-4}
Ultimate strain	κ_u	1.25×10^{-2}
Characteristic length	l	$\sqrt{7 \times 10^{-4}}$ cm

As a first test, a Poisson's coefficient $\nu = 0$ is considered. To assess the regularisation capabilities, the simulation is carried out with four different

meshes of 10×11, 20×21, 30×31 and 40×41 elements, see Figures 11(b)-(e). Note that mesh size and imperfection size insensitivies are analysed simultaneously.

The results are summarised in Figures 12 and 13. The damage distributions of Figure 12 and the force-displacement curves of Figure 13 clearly show that the model is regularised. Figure 12 also shows the crack branching caused by the boundary conditions at the right-hand-side of the specimen.

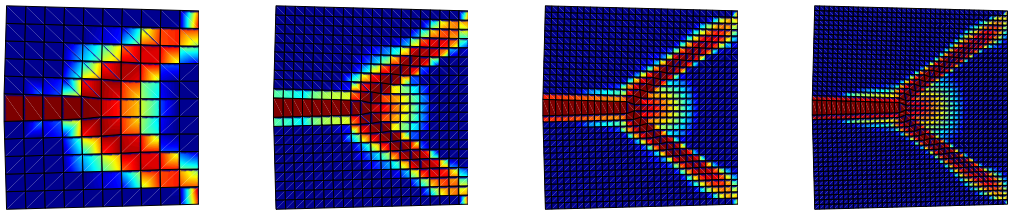

Figure 12: Direct tension test: damage for the four finite element meshes with deformed meshes ($\times 50$)

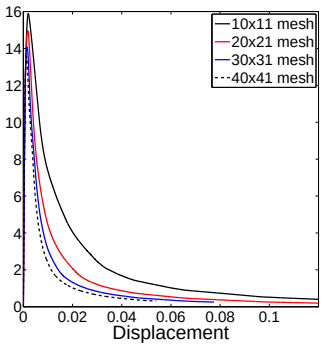

Figure 13: Direct tension test: force-displacement curves for the four finite element meshes

As a second test, the finest mesh of 40×41 elements and four different Poisson's coefficients $\nu = 0$, $\nu = 0.2$, $\nu = 0.25$ and $\nu = 0.3$ are considered. Again, mesh-insensitive results are obtained. Figure 14 shows the influence of ν in the crack pattern: the length of the damaged branch and the initiation of the branching phenomenon strongly depend on the Poisson's ratio.

5.4. Three-point bending test

Together with softening regularisation, non-local models are also expected to capture size effects. To check whether this is the case for the approach

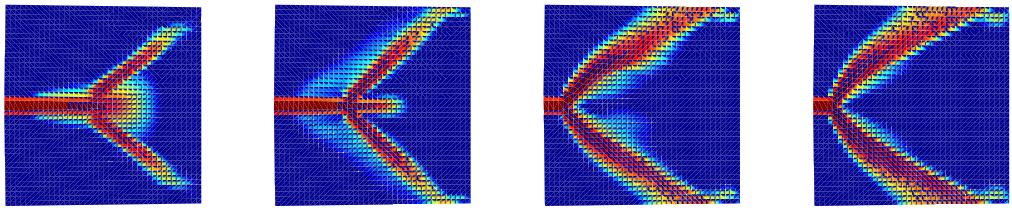

Figure 14: Direct tension test: damage for the four Poisson's coefficients with deformed meshes ($\times 50$)

presented, the three-point bending test reported in Askes et al. (2004) is reproduced here. The beam has dimensions $4D \times D$ and a proportional wedge-shaped notch with dimensions $0.25D \times 0.25D$, see Figure 15(a). Seven different sizes are analysed ($D = 1$, 2, 4, 8, 16, 32 and 64 mm) with a constant internal length scale of $\ell = 0.1$ mm. The damage model given by Equations (14)–(16), with the material parameters of Table 5, are used.

Table 5: Three-point bending test. Material parameters

Meaning	**Symbol**	**Value**
Young's modulus	E	30 000 MPa
Poisson's ratio	ν	0.15
Damage initiation strain	κ_i	0.0001
Post-peak slope parameter	β	500
Compressive-to-tensile strength ratio	k	10
Internal length scale	ℓ	0.1 mm

The results are plotted in Figure 15(b), which shows the nominal strength σ (defined as the peak load divided over the structural dimension D) versus D in the usual log-log scale. Note that a size effect in the whole dimension range is indeed predicted by the numerical experiments, and it is in reasonable accordance with Bažant's Size Effect Law (SEL), given by

$$\sigma = \frac{Bf_t'}{\sqrt{1 + D/D_0}} \tag{74}$$

where parameters Bf_t' (f_t': tensile strength of the material; B: geometry-related parameter) and D_0 (characteristic size) are fitted via linear regression (resulting in $Bf_t' = 0.3287$ MPa and $D_0 = 34.55$ mm).

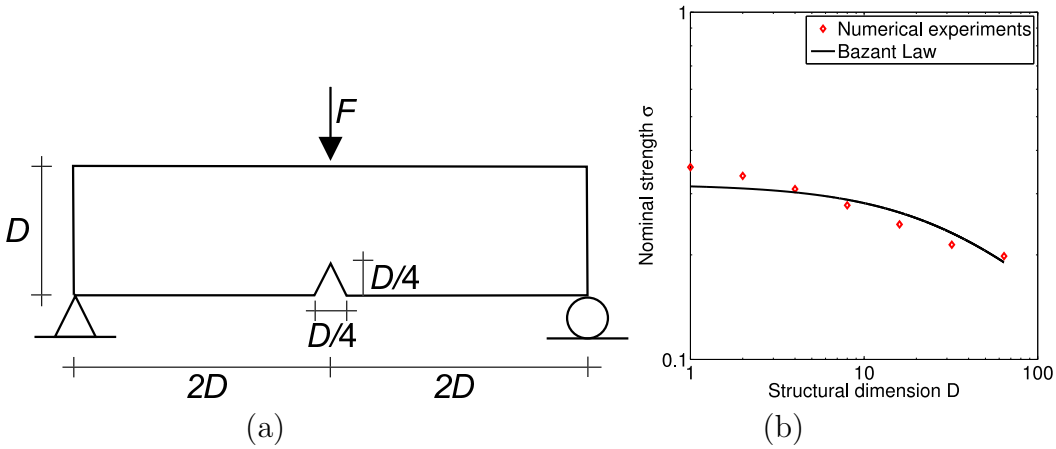

Figure 15: Three-point bending test: (a) problem statement; (b) nominal strength vs. structural dimension

The authors appreciate that the correspondence with SEL is not as strong as perhaps would be expected: the large-size asymptote does not exhibit a slope of -1:2 as predicted by SEL. However, this seems to be quite common: numerical simulations carried out with non-local damage models tend to predict large size asymptotes with less steep slopes, see for instance (Le Bellégo et al., 2003) where an integral nonlocal model was used and (Askes et al., 2004; Iacono et al., 2008) where gradient-type non-locality was used. The results of these studies, alongside those of the present paper, are obtained from various independently developed finite element codes; thus, the observed large-size asymptotes seem to be a property of the non-locality rather than of the particular implementation.

6. CONCLUDING REMARKS

We have presented a general framework for the regularisation of strain-softening continua. Generality stems from the fact that gradient enrichment is introduced at the level of displacements, rather than some (model-dependent) internal variable. This approach does not provide a universal recipe for the formulation of non-local models: as illustrated for plasticity in Sections 2.2.2 and 2.2.3, careful design and analysis of the localisation properties are still required. However, it brings together gradient elasticity (goals of gradient enrichment: removal of singularities and dispersive behaviour) and gradient inelasticity (goals: softening regularisation and description of

size effects). Moreover, working with two displacement fields has attractive features regarding consistent linearisation of the equilibrium equation and the prescription of boundary conditions for the regularisation equation.

The 1D and 2D examples clearly show that mesh sensitivity and imperfection size sensitivity are indeed avoided with the proposed approach. Although simple prototype models have been used (i.e. isotropic damage and Mises plasticity), we conjecture that two displacement fields may also be used to regularise more sophisticated models (for instance, coupling damage and plasticity).

As dictated by the one-dimensional localisation analysis, the gradient enrichment affects only the inelastic part of the stress, whereas the elastic stress remains local. The localisation analysis also provides *i)* insight into the different qualitative behaviour (locking vs. non-locking) of the two plasticity models (non-local plastic strain vs. local/non-local softening variable) and *ii)* an approximation to the width of the localisation zone.

Acknowledgments

We gratefully acknowledge the financial support of the Ministerio de Ciencia e Innovación (grants BIA2007-66965 and DPI2007-62395) and the Engineering and Physical Sciences Research Council (grant EP/E01867X/1).

References

Aifantis, E.C., 1992. On the role of gradients in the localization of deformation and fracture. Int. J. Eng. Sci. 30 (10), 1279–1299.

Aifantis, E.C., 2003. Update on a class of gradient theories. Mech. Mater. 35 (3-6), 259–280.

Altan, S.B., Aifantis, E.C., 1992. On the structure of the mode III crack-tip in gradient elasticity. Scr. Metall. Mater. 26 (2), 319–324.

Amanatidou, E., Aravas, N., 2002. Mixed finite element formulations of strain-gradient elasticity problems. Comput. Methods Appl. Mech. Eng. 191 (15-16), 1723–1751.

Askes, H., Aifantis, E.C., 2002. Numerical modeling of size effects with gradient elasticity — formulation, meshless discretization and examples. Int. J. Fract. 117 (4), 347–358.

Askes, H., Bennett, T., Aifantis, E.C., 2007. A new formulation and C-0-implementation of dynamically consistent gradient elasticity. Int. J. Numer. Methods Eng. 72 (1), 111–126.

Askes, H., Gutierrez, M.A., 2006. Implicit gradient elasticity. Int. J. Numer. Methods Eng. 67 (3), 400–416.

Askes, H., Morata, I., Aifantis, E.C., 2008. Finite element analysis with staggered gradient elasticity. Comput. Struct. 86 (11-12), 1266–1279.

Askes, H., Simone, A., Sluys, L.J., 2004. Modelling of size effect with regularised continua. Acta Polytechnica 44 (5-6), 35–41.

Bažant, Z.P., Jirásek, M., 2002. Nonlocal integral formulations of plasticity and damage: survey of progress. J. Eng. Mech.-ASCE 128 (11), 1119–1149.

Bažant, Z.P., Lin, F.B., 1988. Non-local yield limit degradation. Int. J. Numer. Methods Eng. 26 (8), 1805–1823.

Bennett, T., Gitman, I.M., Askes, H., 2007. Elasticity theories with higher-order gradients of inertia and stiffness for the modelling of wave dispersion in laminates. Int. J. Fract. 148 (2), 185–193.

Chang, C.S., Askes, H., Sluys, L.J., 2002. Higher-order strain/higher-order stress gradient models derived from a discrete microstructure, with application to fracture. Eng. Fract. Mech. 69 (17), 1907–1924.

de Borst, R., Muhlhaus, H.-B., 1992. Gradient-dependent plasticity — formulation and algorithmic aspects. Int. J. Numer. Methods Eng. 35 (3), 521–539.

de Borst, R., Pamin, J., 1996. Some novel developments in finite element procedures for gradient-dependent plasticity. Int. J. Numer. Methods Eng. 39 (14), 2477–2505.

de Vree, J. H.P., Brekelmans, W. A.M., van Gils, M. A.J., 1995. Comparison of nonlocal approaches in continuum damage mechanics. Comput. Struct. 55 (4), 581–588.

Engel, G., Garikipati, K., Hughes, T. J.R., Larson, M.G., Mazzei, L., Taylor, R.L., 2002. Continuous/discontinuous finite element approximations

of fourth-order elliptic problems in structural and continuum mechanics with applications to thin beams and plates, and strain gradient elasticity. Comput. Methods Appl. Mech. Eng. 191 (34), 3669–3750.

Iacono, C., Sluys, L.J., van Mier, J. G.M., 2008. Calibration of a higher-order continuum model using global and local data. Eng. Fract. Mech. 75 (16), 4642–4665.

Jirásek, M., Marfia, S., 2005. Non-local damage model based on displacement averaging. Int. J. Numer. Methods Eng. 63 (1), 77–102.

Jirásek, M., Marfia, S., 2006. Nonlocal damage models: displacement-based formulations. In: Meschke, G., de Borst, R., Mang, H., Bićanić, N. (Eds.), Computational Modelling of Concrete Structures. pp. 381–390.

Jirásek, M., Patzak, B., 2002. Consistent tangent stiffness for nonlocal damage models. Comput. Struct. 80 (14-15), 1279–1293.

Jirásek, M., Rolshoven, S., 2003. Comparison of integral-type nonlocal plasticity models for strain-softening materials. Int. J. Eng. Sci. 41 (13-14), 1553–1602.

Jirásek, M., Rolshoven, S., 2009a. Localization properties of strain-softening gradient plasticity models. part I: Strain-gradient theories. Int. J. Solids Struct. 46 (11-12), 2225–2238.

Jirásek, M., Rolshoven, S., 2009b. Localization properties of strain-softening gradient plasticity models. part II: Theories with gradients of internal variables. Int. J. Solids Struct. 46 (11-12), 2239–2254.

Le Bellégo, C., Dubé, J.F., Pijaudier-Cabot, G., Gérard, B., 2003. Calibration of nonlocal damage model from size effect tests. Eur. J. Mech. A-Solids 22 (1), 33–46.

Mazars, J., 1986. A description of micro- and macroscale damage of concrete structures. Eng. Fract. Mech. 25 (5-6), 729–737.

Muhlhaus, H.-B., Aifantis, E.C., 1991. A variational principle for gradient plasticity. Int. J. Solids Struct. 28 (7), 845–857.

Pamin, J., 1994. Gradient-dependent plasticity in numerical simulation of localization phenomena. Ph.D. thesis, Delft University of Technology.

Ramaswamy, S., Aravas, N., 1998a. Finite element implementation of gradient plasticity models — Part I: Gradient-dependent yield functions. Computer Methods in Applied Mechanics and Engineering 163 (1-4), 11–32.

Ramaswamy, S., Aravas, N., 1998b. Finite element implementation of gradient plasticity models — Part II: Gradient-dependent evolution equations. Comput. Methods Appl. Mech. Eng. 163, 33–53.

Rodríguez-Ferran, A., Morata, I., Huerta, A., 2004. Efficient and reliable nonlocal damage models. Comput. Methods Appl. Mech. Eng. 193 (30-32), 3431–3455.

Rodríguez-Ferran, A., Morata, I., Huerta, A., 2005. A new damage model based on non-local displacements. Int. J. Numer. Anal. Meth. Geomech. 29 (5), 473–493.

Ru, C.Q., Aifantis, E.C., 1993. A simple approach to solve boundary-value problems in gradient elasticity. Acta Mech. 101 (1-4), 59–68.

Shu, J.Y., King, W.E., Fleck, N.A., 1999. Finite elements for materials with strain gradient effects. Int. J. Numer. Methods Eng. 44 (3), 373–391.

Simo, J.C., Hughes, T. J.R., 1998. Computational inelasticity. Springer.

Tang, Z., Shen, S., Atluri, S.N., 2003. Analysis of materials with strain-gradient effects: a Meshless Local Petrov-Galerkin (MLPG) approach, with nodal displacements only. CMES-Comp. Model. Eng. Sci. 4 (1), 177–196.

Tenek, L.T., Aifantis, E.C., 2002. A two-dimensional finite element implementation of a special form of gradient elasticity. CMES-Comp. Model. Eng. Sci. 3 (6), 731–741.

Vermeer, P.A., Brinkgreve, R. B.J., 1994. A new effective non-local strain-measure for softening plasticity. In: Chambon, R., Desrues, J., Vardoulakis, I. (Eds.), Localisation and Bifurcation Theory for Soils and Rocks. Balkema, Rotterdam, pp. 89–100.

Zervos, A., 2008. Finite elements for elasticity with microstructure and gradient elasticity. Int. J. Numer. Methods Eng. 73 (4), 564–595.